Precast tunnel segments with GFRP reinforcement

CrossMark

Angelo Caratelli, Alberto Meda, Zila Rinaldi *, Simone Spagnuolo

University of Rome "Tor Vergata", Italy

A B S T R A C T

The possibility of substituting the traditional steel reinforcement with Glass Fiber Reinforced Polymer (GFRP) bars in precast segmental lining tunnels is investigated herein.

The use of this kind of reinforcement in tunnel segments allows several advantages mainly related to durability aspects or when provisional lining is forecast. Furthermore, GFRP reinforcement can be used when dielectric joints are necessary.

In the presented research, full-scale bending tests have been performed on precast segments in order to compare the structural performance of GFRP reinforced concrete with respect to traditional steel reinforced concrete. Furthermore, peculiar aspects of the design procedure for the proposed solution are remarked and discussed.

© 2016 Elsevier Ltd. All rights reserved.

1. Introduction

The use of Glass Fiber Reinforced Polymer (GFRP) rebars in concrete structures is an innovative solution that can be proposed in alternative to the traditional steel rebars, mainly when a high resistance to the environmental attack is required. Indeed, in comparison with steel, GFRP does not suffer corrosion problems, presents higher tensile capacity, and lower weight (Nanni, 1993; Benmokrane et al., 1995; Alsayed et al., 2000). The material is also non-conductive for electricity and non-magnetic. Nevertheless, it has to remark that this type of reinforcement is not suitable for all the applications. Firstly, the cost of the GFRP rebars is generally higher with respect to the traditional steel ones, moreover the GFRP reinforcement is affected by problems related to static fatigue when subjected to high-level long-term tensile stresses (Almusallam et al., 2006). Furthermore, the structural effects of the low value of the Young's modulus and the bond behaviour (Cosenza et al., 1997; Yoo et al., 2015) have to be considered. Finally, the durability performance of GFRP bars could be improved by selecting the appropriate constituents of the composites (Micelli and Nanni, 2004; Chen et al., 2007).

The possibility of using a GFRP reinforcement in precast tunnel segments is investigated herein. In mechanical excavated tunnels, generally made with a Tunnel Boring Machine (TBM), the lining is composed of precast elements, placed by the TBM during the exca-

vation process and used as reaction elements during the advancing phase.

The adoption of precast segments reinforced with GFRP rebars is suitable when durability problems could jeopardize the tunnel integrity (e.g. aggressive environmental as in waste water tunnels or presence of aggressive soils). Furthermore, the possibility of using non-metallic reinforcement allows a strong reduction of the concrete cover, avoiding problems of crushing during the segments handling. The GFRP reinforcement is also suitable in parts of the tunnel that have to be eventually demolished. Typical examples are metro or railways lines, when the station is built after the tunnel excavation or in road tunnels when the section of the tunnel has to be modified for creating safety areas. Finally, the use of this technology is adequate for creating dielectric joint in tunnels.

The adoption of GFRP rebars in substitution to traditional steel cage can be proposed in a series of tunnels affected by the aforementioned problems. The higher cost of the material, with respect to traditional steel cages, can be balanced if the overall costs related to the tunnel construction and maintenance is considered. Furthermore, the lining at final stage is often mainly in compression and the static fatigue in the GFRP rebars is limited.

On the structural point of view it is important to demonstrate to the designers that the behaviour of precast tunnel segments reinforced with GFRP rebars is comparable (or even better) with respect to the traditional steel reinforcement. With this purpose, full-scale tests on precast segments subjected to bending actions have been performed in order to compare the structural behaviour of elements reinforced with GFRP and traditional steel bars. Further full-scale tests have been performed with the aim to verify

---

* Corresponding author at: Department of Civil Engineering and Computer Science, University of Rome Tor Vergata, Via del Politecnico, 1, 00133 Rome, Italy.
  E-mail address: rinaldi@ing.uniroma2.it (Z. Rinaldi).

the structural behaviour under TBM load actions. Finally, some considerations on the design of precast segments with GFRP reinforcement are presented.

2. Description of the experimental campaign

Two full-scale segments were tested in the Laboratory of the University of Rome Tor Vergata: a reference one reinforced with ordinary steel rebars (named SR) and a segment reinforced with GFRP rebars (named GFR). Both the specimens are characterized by a thickness of 400 mm, a length of about 4150 mm and a width of about 1483 mm (Fig. 1).

The segments were subjected to bending actions in order to highlight the effect of the reinforcement. Bending test is also representative of the provisional loading stages as demoulding, storage and handling.

The reference segment has been cast with a traditional steel cage made of 12Ø12 bars placed in the intrados and 12Ø12 bars at the extrados surfaces (Fig. 2a). The steel rebars are classified, according to EC2 (EN-1992-1, 2008), as B500 with characteristic

yielding stress (f_{yk}) equal to 500 MPa. The GFR segment is reinforced with GFRP bars with a characteristic tensile strength (f_{tk}) equal to 690 MPa. In particular, the reinforcement consists in 12Ø12 longitudinal bars at the extrados surface and 12Ø14 longitudinal bars at the intrados surface (Fig. 2b). The assembled cage is shown in Fig. 3. The two segments were cast with concrete coming from the same batch. A C40/50 concrete was used, with an average cubic strength equal to 61 MPa.
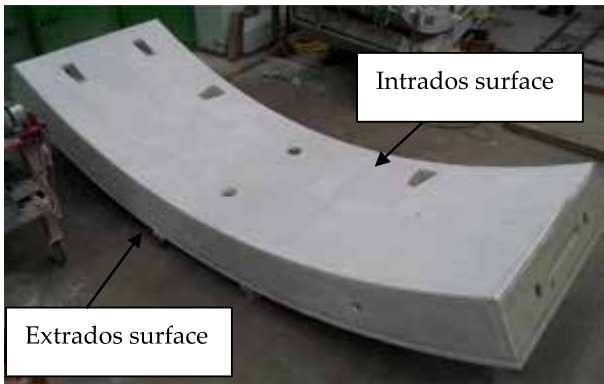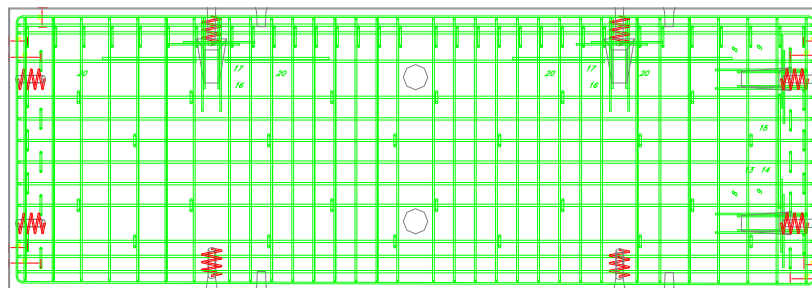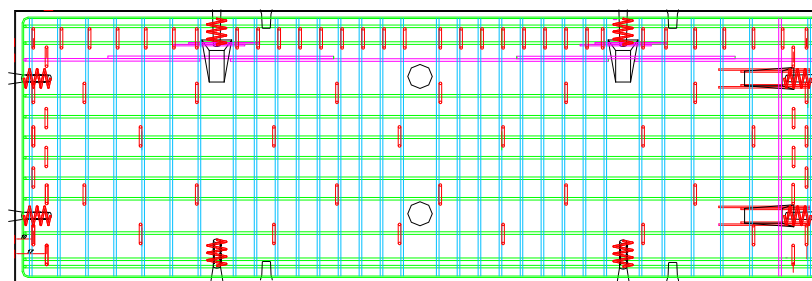

Fig. 3. GFRP cage.

Table 1
Design values of the material properties for the M-N envelopes definition.

Material	Characteristic values	Safety coefficients	Design values
Concrete C40/50	f_{ck} = 40 MPa	γ_c = 1.5; α_c = 1	$f_{cd} = \frac{f_{ck} \cdot \alpha_c}{\gamma_c} = 26.7$ MPa
Steel	f_{yk} = 500 MPa	γ_s = 1.15	$f_{yd} = \frac{f_{yk}}{\gamma_s} = 435$ MPa
GFRP	f_{tk} = 690 MPa	η_a = 0.7; η_l = 1;	$f_{td} = \frac{f_{tk} \cdot \eta_a \cdot \eta_l}{\gamma_f} = 322$ MPa
	$\varepsilon_{fk} = \frac{f_{tk}}{E_f} = 1.64\%$[a]	γ_f = 1.5 α = 0.9	$\varepsilon_{fu} = \alpha \frac{\varepsilon_{fk} \cdot \eta_a}{\gamma_f} = 0.69\%$

[a] E_f = 42 GPa (mean value).

Fig. 1. Tunnel segment.

Fig. 2. Detailing for the traditional reinforcement (a) and the GFRP reinforcement (b).
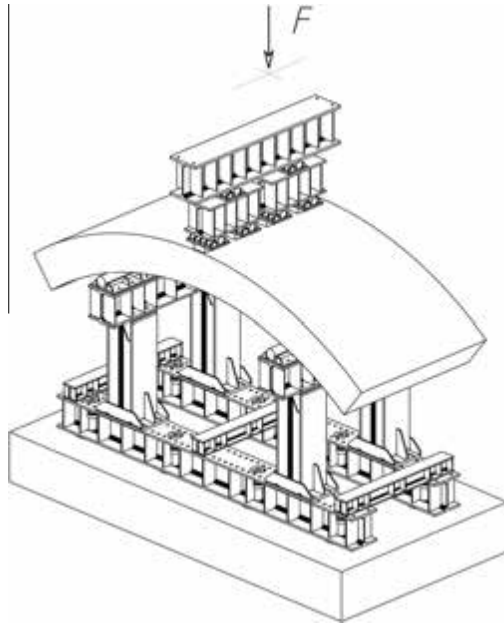
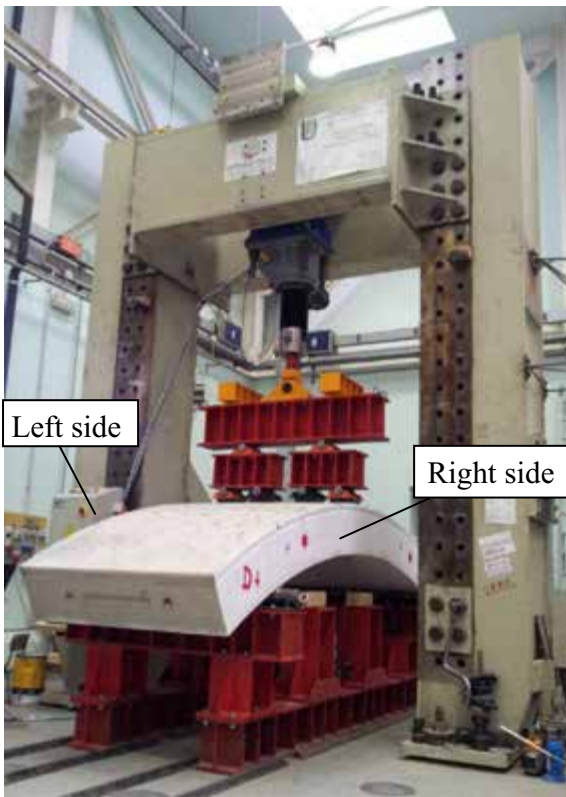Fig. 4. Bending test set-up: scheme (Caratelli et al., 2012).
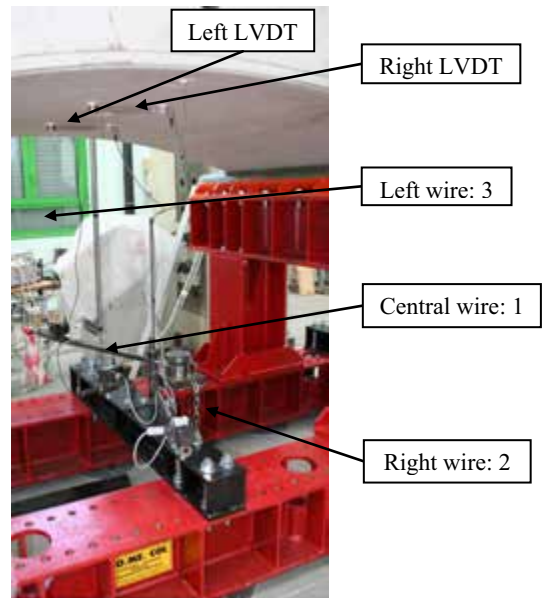

Fig. 5. Bending tests.
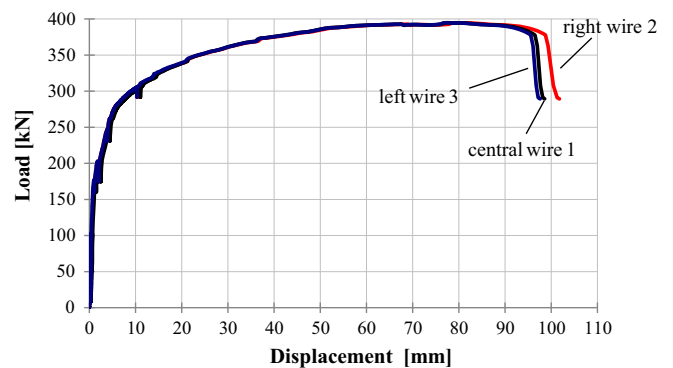

Fig. 6. Bending test instrumentation.

Fig. 7. Segment SR: load-displacement diagram.

The GFRP reinforcement has been designed, according to the codes indications (Fib Bulletin 40, 2007; CNR-DT203, 2007), in order to provide the same ultimate bending resistance of the reference SR segment. The characteristic and design properties of the materials, used for the evaluation of the ultimate bending moments of GFR and SR elements, are summarised in Table 1.

With reference to the concrete in compression, the safety coefficient (γ_c) is assumed equal to 1.5, according to (EN-1992-1,

2008); the long term behaviour factor α_c is set equal to 1 (EN-1992-1, 2008). For what the reinforcement is concerned, it is worth remarking the different value of the safety coefficient, adopted in the design, equal to 1.15 (γ_s) and 1.5 (γ_f) for the steel reinforcement and for GFRP rebars, respectively. Furthermore, in order to account for the possible degradation of the GFRP mechanical properties under specific environmental conditions, such as exposition to moisture, typical of tunnel linings, the environmental conversion factor (η_a) is applied, ad set equal to 0.7 according to (CNR-DT203, 207). The conversion factors for long-term effects (η_l), accounting for possible degradation of the GFRP mechanical properties due to creep, relaxation, and fatigue, is set equal to 1, as suggested in (CNR-DT203, 2007), for Ultimate Limit State analyses.

The bending tests were performed with the loading set-up illustrated in Figs. 4 and 5, in displacement control, under a reacting frame of 4000 kN. A close loop 1000 kN electromechanical jacket was adopted, with a stroke speed of 10–16 μm/s.

The following phases were followed:

1. Segment placement on the boundary system;
2. Assembling of the loading distribution system;
3. First loading-unloading cycle up to 20 kN;
4. First loading-unloading cycle up to 100 kN;
5. Loading cycle up to the segment cracking;
6. Displacement increase up to the segment failure. Intermediate loading steps were further performed for the survey of the cracking pattern, as shown in the following.

The segments were placed on cylindrical support with a span of 3000 mm and the load, applied at midspan, was transversally distributed by adopting a steel beam as shown in Fig. 5.
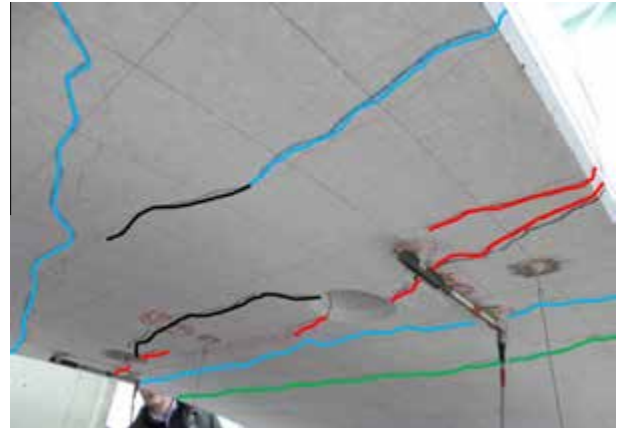

Fig. 10. Segment SR: load level of 300 kN - intrados surface.

Fig. 11. Segment SR: load level of 300 kN, maximum crack width (lateral surface).
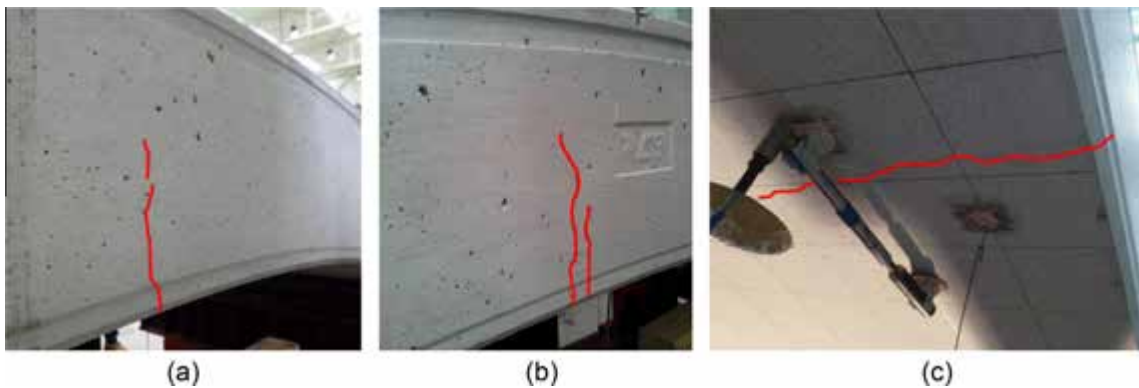

Fig. 8. Segment SR: load level of 175 kN; (a) left lateral surface and (b) right lateral surface, intrados surface.
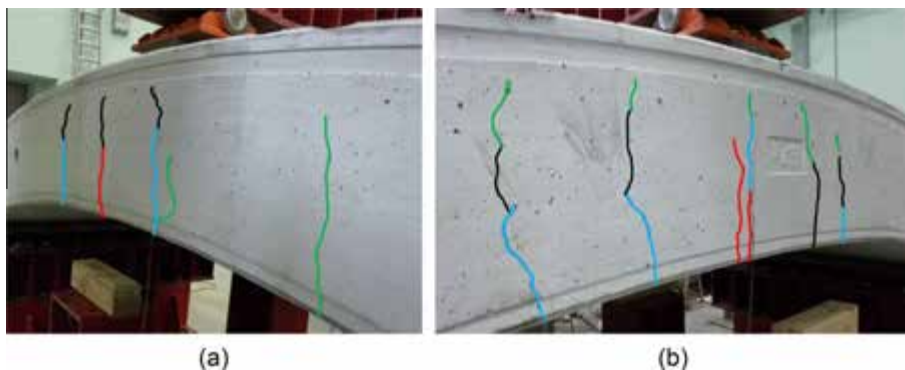

Fig. 9. Segment SR: load level of 300 kN; (a) left lateral surface and (b) right lateral surface.

Fig. 12. Segment SR: failure stage (a) left lateral surface and (b) right lateral surface.

During the test, were continuously registered:

- the load, measured with a 1000 kN load cell with a precision of 0.2%;
- the midspan displacement, measured with three potentiometer wire transducers placed along the transverse line (Fig. 6);
- the crack opening at midspan, measured with two Linear Variable Displacement Transducers - LVDTs - (Fig. 6).

Furthermore, the crack pattern was recorded at different steps, with the help of a grid (100 × 100 mm) plotted on the intrados surface.

3. Test results

3.1. Bending test on the segment SR

Bending test results on segment SR, with traditional steel reinforcement, are here summarised. The load – displacement relationship measured by the wire transducers (Fig. 6) is plotted in Fig. 7. It is worth noting that the three instruments, located in the midspan, measured almost coincident displacement values, highlighting a homogeneous behaviour of the segment in this direction. The maximum load is equal to about 395 kN. The first cracks opened for a load value of about 175 kN, close to the midspan of the segment on the lateral and intrados surfaces (Fig. 8). Two further cracks, almost symmetrical with respect to the midspan, crossing both the intrados and lateral surfaces, opened for a load level of about 200 kN (Fig. 14). A further crack diffusion took place for the following steps, with the formation of new cracks and the lengthening and widening of the already formed ones.

As an example, the crack distribution for a load level of 300 kN is highlighted in Figs. 9 and 10 for the lateral and intrados surfaces, respectively. At this stage, the maximum crack width was equal to about 3 mm, as shown in Fig. 11. The collapse was due to the rebars failure, highlighted by the great widening of two main cracks, as clearly visible in Figs. 12 and 13, where the ultimate state is shown. The final crack pattern, at the end of the test is finally summarised in Fig. 14.

The crack width is further evaluated with the two LVDTs measures, plotted in Fig. 15 versus the load. It is worth remarking the measured values refer to the one main crack that gets across the instruments (Fig. 14).
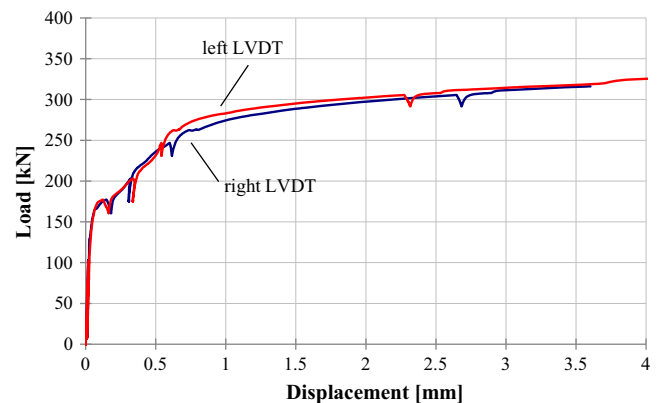

Fig. 13. Segment SR: failure stage - intrados surface.

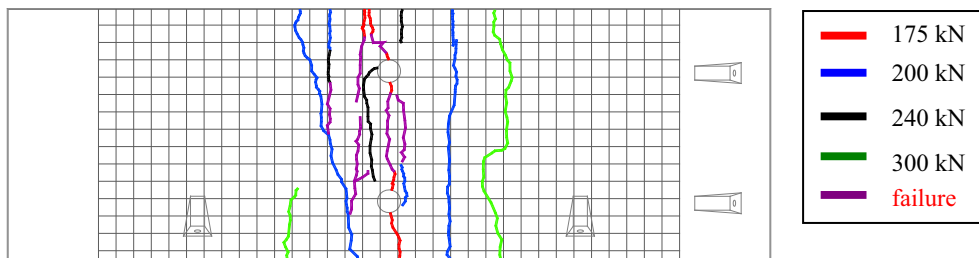**Fig. 15.** Segment SR. Load-displacement diagram (LVDTs).

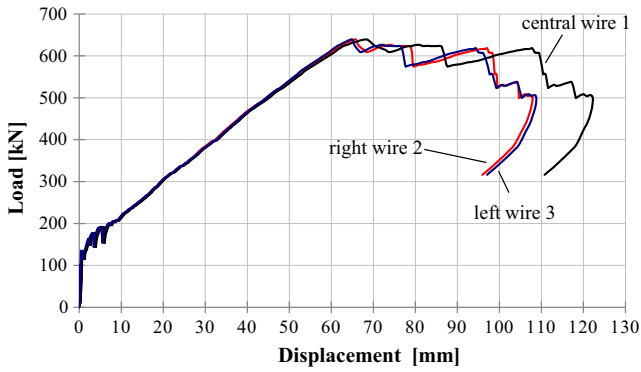**Fig. 14.** Segment SR: final crack pattern.

Fig. 16. Segment GFR: load-displacement diagram.

3.2. Bending test on the segment GFR

The main results of the bending test on the segment GFR, with GFRP bars, are here reported.

The load – displacement relationship related to the wire transducers (Fig. 6) is plotted in Fig. 16.

Again, the three instruments, located in the midspan, measured very similar displacement values, with a homogeneous behaviour of the segment in this direction. The maximum load is equal to about 640 kN.

The first crack opened for a load value of about 130 kN close to the midspan of the segment on the lateral and intrados surfaces (Figs. 17 and 18). A lengthening and widening of the already formed crack took place for a load level of 135 kN, while a new crack, crossing the intrados side and reaching the lateral surfaces,

Fig. 17. Segment GFR: load level of 130 kN; (a) left lateral surface and (b) right lateral surface.

Fig. 18. Segment GFR: load level of 130 kN. Intrados surface: (a) left side and (b) right side.

Fig. 19. Segment GFR: load level of 195 kN; (a) left lateral surface and (b) right lateral surface.

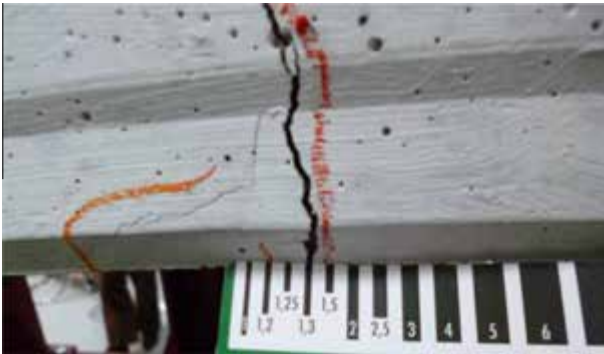**Fig. 20.** Segment GFR: load level of 195 kN - intrados surface.

Fig. 21. Segment GFR: load level of 195 kN, maximum crack width.

appeared for load levels of 160 kN, again close to the midspan (Fig. 24).

When the load was increased, up to 175 and 195 kN, two almost symmetrical cracks formed, 40–50 cm away from the midspan at the intrados surface, reaching the lateral surfaces. The crack distribution on the lateral and intrados surfaces, for a load level of 195 kN is highlighted in Figs. 19 and 20. At this stage, the maximum crack width was equal to about 1.3 mm, as shown in Fig. 21. Afterwards, a quick diffusion of the crack distribution took place. Different cracks opened almost parallel to the already formed ones, up to the segment collapse due failure of the rebars, highlighted also by the load drops in the measured load-displacement graph (Figs. 16 and 25). Finally, fourteen cracks, about 100 mm spaced, were detected at the intrados surface (Fig. 24).

The crack pattern related to the ultimate state is shown in Figs. 22 and 23. The final crack pattern, at the end of the test is summarised in Fig. 24.

Fig. 23. Segment GFR: failure stage - intrados surface.

Unfortunately, the LVDTs were soon detached (for a crack passing through their supports) and their measures were not recorded.

4. Comparisons and design consideration

The results expressed in terms of load versus midspan displacement, obtained by the two performed full-scale tests are compared in Fig. 25. The main experimental outcomes are summarised in Table 2. As already mentioned, the first crack occurred for a load level of 175 kN and 130 kN for the SR and GFR segments, respectively. Eventually, in both the elements several cracks developed. It can be noticed that the SR specimen showed a stiffer behaviour compared to the GFR segment. This was mainly due to the higher bond of traditional rebars with respect to the GFRP ones. This aspect is also confirmed by the crack pattern for different load levels (Fig. 24), since more cracks are present in the GFR segment. Despite the brittleness of the reinforcement, the structural behaviour of GFR was anyway ductile, with an ultimate displacement comparable (and even slightly higher) to what obtained for SR segment (see Table 2).

Looking at the maximum bearing capacity, it can be noticed a higher failure load for the GFR segment. This is due to the different safety coefficients adopted in the design for the two materials (1.15 for the steel reinforcement and 1.5 for GFRP rebars) and to the differences between their nominal characteristic strength as compared to their mean experimental values. In order to clarify this aspect and discuss better the experimental results, some considerations have to be done on the design of concrete segments reinforced with GFRP bars, with respect to steel reinforced ones.

Bending moment – axial force (M-N) interaction envelopes have been drawn in order to compare the sectional behaviour of the two considered solutions. Design guidelines for GFRP rebars (fib bulletin 40, ACI 440, CNR DT203) suggest using elasto-brittle behaviour in tension and no resistance in compression.

Initially, the design strength values of the materials (Table 1) are adopted (i.e. considering the characteristic nominal value of the strength divided by the material safety coefficient). The

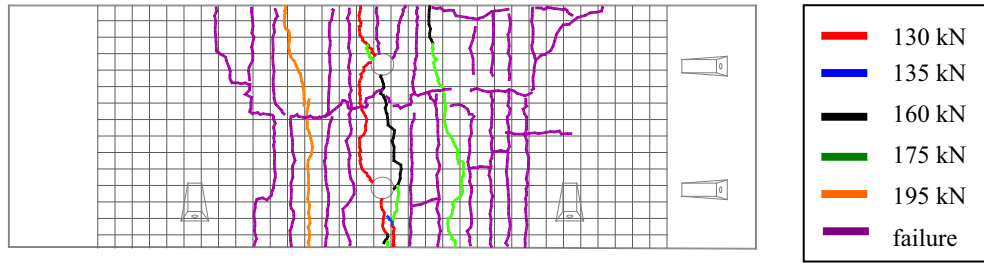**Fig. 22.** Segment GFR: failure stage - right lateral surface.
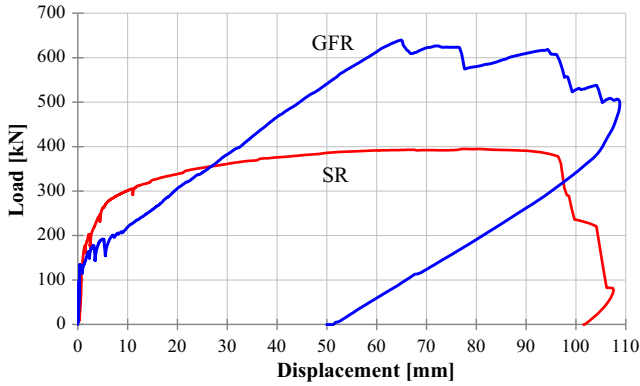
Fig. 24. Segment GFR: final crack pattern.

Fig. 25. Load versus midspan displacement curves. Comparisons.

Table 2
Experimental results.

Reinforcement	Flexural failure mode	Pmax (kN)	δ_1[a] (mm)	δ_{max}[b] (mm)
Steel	Rebars rupture	395	10.6	78.4
GFRP	Rebars rupture	640	65.2	103

  [a] δ_1: displacement related to steel yielding in SR and to stiffness drastic variation in GFR segment.
  [b] δ_{max}: max displacement in SR; evaluated at 0.85 Max Load in GFR segment.
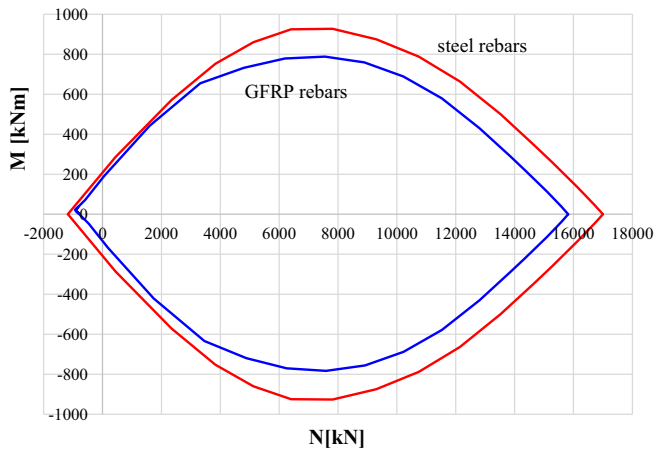

Fig. 26. Bending moment versus axial force envelope for the two tested segment, evaluated considering the design strength of the materials.

concrete in compression is simulated with a classical stress-block behaviour, a linear behaviour is assumed for the GFRP rebars and a typical elasto-plastic relationship is considered for the steel rebars. The classical section hypotheses of Bernoulli's strain

linearity, and perfect bond between concrete and reinforcement are assumed. The design M-N interaction envelopes for the section of both the GFR and SR segments are compared in Fig. 26. It can be clearly noted the attainment of the same bearing capacity of the steel reinforced element, at least in pure bending, assumed as design criterion for the reinforcement of the GFR segment.

Eventually the mean values of the strength properties (measured with tests) are considered and the safety coefficients are assumed all equal to one. The adopted properties are summarised in Table 3 and the actual interaction envelopes, evaluated with the mean experimental values of the strength, are shown in Fig. 27. In the same figure the bending moment measured in the experimental tests, described in Section 3, are further superimposed.

Since the dots lie very close to the related envelops, the simplified check procedure with M-N envelopes, and the adopted hypotheses on the constitutive relationship of the materials, appear suitable for foreseeing the actual bearing capacity. Furthermore, as already mentioned, it can be clearly observed, how the adoption of average values of the material strength (without any

Table 3
Experimental mean values of the material properties for the M-N envelopes definition.

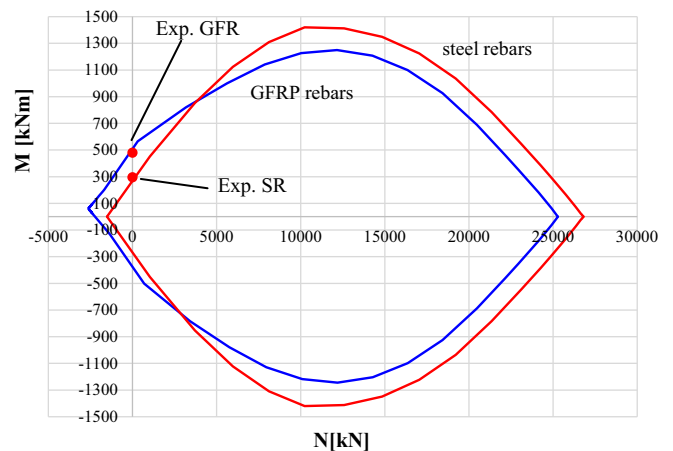| Material	Experimental mean values
Concrete	R_{cm} = 61 MPa; f_{cm} = 0.83 R_{cm} = 50.6 MPa
Steel	f_{ym} = 600 MPa
GFRP	f_{tm} = 844 MPa $\varepsilon_{fk} = \frac{f_{tk}}{E_f}$ = 2%[a]

  [a] E_f = 42 GPa (mean value).

Fig. 27. Bending moment versus axial force envelope for the two tested segment, evaluated considering the average strength of the materials.

safety coefficient) leads to highest bearing capacity of the segment with GFRP bars, as evidenced in the full scale tests.

5. TBM thrust test

In order to verify the behaviour of segments reinforced with GFRP bars under the TBM thrust action, a further full-scale test has been performed. A testing system developed in the Testing Laboratory of the University of Rome Tor Vergata has been used (Meda et al., 2011; Caratelli et al., 2012). In this case, a segment with a thickness of 250 mm has been adopted (Fig. 28). The element is reinforced with a GFRP cage, made of 13+13Ø14 longitudinal bars, 13+13Ø12 straight crossbars and 42Ø14 brackets hoops on the perimeter (Fig. 28) with minimum cover of 15 mm. The segment was cast with concrete characterized by a mean cubic strength equal to 61.7 MPa.

Fig. 29 shows the testing system adopted. In the considered configuration, the system is able to apply up to 4000 kN on a single pad.

In order to reproduce the field condition, in the experimental set-up two hydraulic jacks act on every steel pad. Every jack, having a loading capacity of 2000 kN, is inserted in a close ring frame made with HEM 360 steel beams and 50 mm diameter Dywidag bars. The segment is placed on a reinforced concrete beam with a 800×800 mm cross section, internal to the close ring frames

(Fig. 29), suitably designed in order to simulate the stiffness of the already placed ring. A hydraulic control system has been adopted with the aim of applying the loads similarly to what happens with the TBM. In particular, it is possible to control the load on a single couple of jackets acting on a single pad. Furthermore, valves able to maintain a constant value of the oil pressure in the circuits have been used. The loads applied on the segment are measured by means of two pressures transducers, each for every couple of jackets.

The vertical displacements of the steel pads are measured with four potentiometric wire transducers, two placed on the front side (intrados) and two on the rear side (extrados) of the segment (Fig. 29). Furthermore, one LVDT is applied between the load pads, at the top (Fig. 29), for measuring the crack opening. All the data are continuously recorded by an acquiring digital system and transmitted to a PC.

Two complete loading – unloading cycles have been carried out, and in particular:

– first cycle: 0–1130 kN (maximum TBM thrust);
– second cycle: 0–2500 kN.

The first crack appeared between the loading pads at the top of the intrados surface, in the LVDT's length, for a load level of about 785 kN (for each pad), and passes through the segment thickness.

Fig. 28. Segment geometry for the TBM thrust test.

Fig. 29. Testing system.

Fig. 30. First cycle. Load step 1130 kN (for each shoe); (a) intrados surface and (b) top surface.

Fig. 31. First cycle. Maximum crack width (1130 kN).

The crack pattern at a load level of 1130 kN, corresponding to the maximum thrust of the considered TBM, is shown in Fig. 30. The maximum crack opening was about 0.05 mm (Fig. 31). The segment was then unloaded and a substantial crack closure was evidenced.

A second load cycle was applied up to a maximum level of 2500 kN (for each pad). The crack between the pads extended up to the extrados surface, as shown in Fig. 32, with a maximum crack width of 0.35 mm (Fig. 33a). The load was removed with a residual crack opening of 0.05 mm (Fig. 33b). The test outcome can be considered very satisfactory, since this maximum crack width was lower than that allowed by the codes for GFRP rebars, typically equal to 0.5 mm (JSCE, 1997; CSA, 2002; ACI 440R-06, 2006; CNR-DT203, 2007). This limit value was never reached during the test. Finally, the first cracking load and the cracks position are
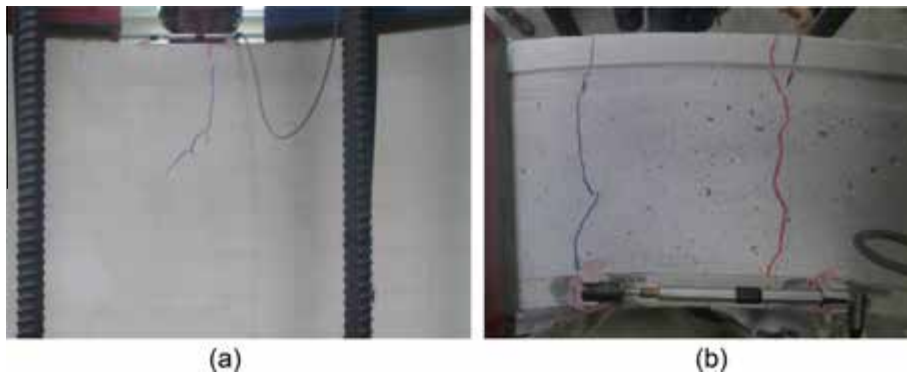

Fig. 32. Second cycle. Load level 2500 kN. (a) Intrados face and (b) top surface.

Fig. 33. Second cycle: maximum crack width; (a) load level 2500 kN; (b) complete unloading.

comparable and consistent with the ones detected in ordinary reinforced concrete segments, as witnessed by other experimental tests, discussed in Meda et al. (2016). A higher value of crack width, but always lower than the limits suggested by the codes, could be measured in GFRP segments with respect to traditionally reinforced segments. This phenomenon is not a cause of concern, since the GFRP reinforcement is not affected by corrosion decay, and, indeed, the code limit for crack width in GFRP reinforced elements is higher than that of steel reinforced ones. Finally, it is worth remarking that the TBM thrust is a temporary action, and in the performed test, the cracks were practically closed after the complete unloading.

6. Conclusions

GFRP rebars can be a solution in some problems that can arise in the segmental lining construction. The suitability of this technique was investigated with full-scale tests and the obtained results allow drawing the following remarks:

- on the point of view of the flexural structural behaviour, there are not significant differences when the steel reinforcement is substituted with a GFRP reinforcement. In fact, despite the brittleness of the material, the performed flexural full-scale test showed that the structure exhibited not only a significant strength but also an adequate ductility;
- the segments reinforced with GFRP bars tested under TBM thrust loads exhibited a suitable behaviour. The maximum crack widths, even under exceptional loads, were always lower than the allowable ones given by the codes;
- the design approach suggested by the codes appears in accordance with the tests evidences. Nevertheless, the adoption, for the GFRP, of safety coefficients remarkably on the safe side, can lead to a structural over-strength, that could be penalizing, mainly for temporary structures.

Finally, the use of GFRP reinforcement appears a very interesting and promising solution in tunnel segmental lining, in some critical situations that often are present in tunnel construction. The choice of adopting GFRP reinforcement instead of a typical steel one, can be particularly advantageous when durability problems are foreseen, for provisional elements to be eventually demolished, and when the necessity of creating dielectric joint in tunnels arises.

References

ACI, 2006. ACI 440.1R-06 – Guide for the Design and Construction of Concrete Reinforced With FRP Bars. ACI Committee 440. American Concrete Institute.

Almusallam, T.H., Al-Salloum, Y.A., 2006. Durability of GFRP rebars in concrete beams under sustained loads at severe environments. J. Compos. Mater. 40 (7), 623–637.

Alsayed, S.H., Al-Salloum, Y.A., Almusallam, T.H., 2000. Performance of glass fiber reinforced plastic bars as a reinforcing material for concrete structures. Composite: Part B 31, 555–567.

Benmokrane, B., Chaallal, O., Masmoudi, R., 1995. Glass fibre reinforced plastic (GFRP) rebars for concrete structure. Constr. Build. Mater. 9 (6), 353–364.

CAN, CSA-S806-02, 2002. Design and Construction of Building Components with Fiber Reinforced Polymers. Canadian Standards Association, Toronto, Ontario, Canada.

Caratelli, A., Meda, A., Rinaldi, Z., 2012. Design according to MC2010 of a fibre-reinforced concrete tunnel in Monte Lirio, Panama. Struct. Concr. 13 (3), 166–173.

Chen, Y., Davalos, J.F., Kim, H.-Y., 2007. Accelerated aging tests for evaluations of durability performance of FRP reinforcing bars for concrete structures. Compos. Struct. 78, 101–111.

CNR DT 203-2006, 2007. Guide for the Design and Construction of Concrete Structures Reinforced With Fiber-Reinforced Polymer Bars. CNR Italian National Research Council.

Cosenza, E., Manfredi, G., Realfonzo, R., 1997. Behavior and modeling of bond of FRP rebars to concrete. J. Compos. Constr. ASCE 1 (2), 40–51.

EN 1992-1, 2008. Eurocode 2. Design of Concrete Structures – General Rules and Rules for Buildings.

fib Bulletin 40, 2007. FRP reinforcement in RC structures Fédération Internationale du Béton (fib), Lausanne, Switzerland.

JSCE, 1997. Recommendation for Design and Construction of Concrete Structures Using Continuous Fibre Reinforcing Materials. Research Committee on Continuous Fiber Reinforcing Materials. Japa Society of Civil Engineering, Tokyo, Japan.

Meda, A., Nerilli, F., Rinaldi, Z., Cignitti, F., Sorge, R., 2011. Numerical analysis of precast tunnel segmental lining supported by full-scale experimental tests. TC28 – 7th Int. Symposium on Geotechnical Aspects of Underground construction in soft ground, Rome (16–18 May).

Meda, A., Rinaldi, Z., Caratelli, A., Cignitti, F., 2016. Experimental investigation on precast tunnel segments under TBM thrust action. Eng. Struct. 119, 174–185.

Micelli, F., Nanni, A., 2004. Durability of FRP rods for concrete structures. Constr. Build. Mater. 18, 491–503.

Nanni, A. (Ed.), 1993. Fiber-Reinforced-Plastic (GFRP) Reinforcement for Concrete Structures: Properties and applications. Developments in Civil Engineering, vol. 42. Elsevier Science, p. 450.

Yoo, D.-Y., Kwon, K.-Y., Park, J.-J., Yoon, Y.-S., 2015. Local bond-slip response of GFRP rebar in ultra-high-performance fiber-reinforced concrete. Compos. Struct. 120, 53–64.